Proceeding South East Asian Conference
on Mathematics and its Application (SEACMA 2013) ISBN 978-979-96152-8-2

Numerical simulation of linear water waves using Smoothed Particle Hydrodynamics

Rizal Dwi Prayogo[1], Leo Hari Wiryanto

Faculty of Mathematics and Natural Sciences, Institut Teknologi Bandung
Jalan Ganesha 10 Bandung, Indonesia
[1]rizal_dp@arc.itb.ac.id

Abstract. In this paper we use Smoothed Particle Hydrodynamics (SPH) method for simulating water waves propagation. Water waves are generated by flap type wavemaker and measurements are taken for some variables. The purposes are to study the characteristics of flap type wavemaker and the behaviors of the water waves by governing different parameters. Wave elevation profiles, wave amplitude, wave period, and wavelength are studied for some cases depending on changes in variable water depth, flap period, flap stroke amplitude, and other variables. In order to examine the accuracy of the model, the numerical results were validated using wavemaker theory and linear wave theory and compared to the analytical solutions. It has been observed that the SPH method are in good agreement with wavemaker theory and linear wave theory. The numerical results of the SPH method agree with the analytical solutions.

Keywords: Flap type wavemaker, linear wave theory (LWT), numerical wave tank (NWT), shallow water waves, Smoothed Particle Hydrodynamics (SPH), wavemaker theory (WMT).

1 Introduction

The study of water wave is very important in the field of marine hydrodynamics to estimate the hydrodynamic force, motion analysis, and wave pattern [1]. In hydrodynamics, the behaviors of water wave are experimentally observed in a rectangular tank. A flap type wavemaker is introduced to generate the desired wave. However, as the development in computational fluid dynamics (CFD), the experimental results can be provided by the numerical model. The numerical model that is used to model wave tank are known as numerical wave tank (NWT) [2].

Some researchers have considered computational approaches for analyzing water wave behaviors. Lal and Elangovan [1] studied the CFD simulation of linear water waves using finite volume package and their results have been confirmed by Finnegan and Goggins [2]. Those results used numerical calculations based on grid. Since the use of grids is not flexible when dealing with free surface flows, particle method has been used as an alternative method. In this paper, we use particle method, i.e. Smoothed Particle Hydrodynamics (SPH) which is a mesh-free Lagrangian method and well-suited for the simulation of complex and free surface flows.

In the SPH method, fluid is represented by a set of arbitrary distributed particles or nodes that posses individual material properties and move according to the governing equation in all kinds of boundaries and interfaces [3]. The SPH method was originally used to model astrophysical problems by Lucy [4] and Gingold and Monaghan [5]. The problem studied here is to develop the research by [1] and [2] using the SPH method.

In this paper, we apply the SPH method for simulating water waves propagation in a NWT. Flap type wavemaker is selected to generate the desired incident waves. The aims are to study the characteristics of flap type wavemaker and the behaviors of water waves by governing parameters. Consider a NWT whose dimension was taken as an experimental wave tank. Generated wave profiles, wave amplitude, wave period, and wavelength were studied for various cases depending on changes in variable water depth, flap period, flap stroke length, and other variables. In order to show the accuracy of the model, we validate the SPH method in two ways, i.e. the generated waves are compared to wavemaker theory (WMT) and the wave elevation is compared to linear wave theory (LWT). The numerical results of the SPH method are also compared to the analytical solutions.

2 Problem Formulation

This section describes the governing equations for linear wave theory and the assumptions made are discussed. We consider a NWT and a flap type wavemaker is selected to generate the desired waves.

2.1 Governing Equations

Consider a case where the waves propagate along x-axis only and the motion is two dimensional in the xy-plane. Let $\mathbf{u}(\mathbf{r}, t)$ be the velocity field of the flow over flat bed. Let $h > 0$ be the still water level (SWL) and $y = \eta(x, t) + h$ be the surface wave elevation. The illustration is shown in Fig. 1.

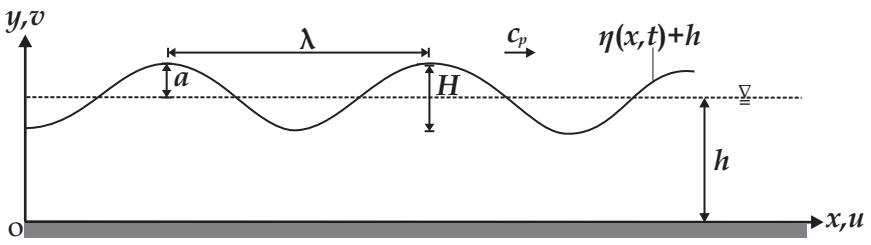

Fig. 1: Sketch of the coordinates and the waves over flat bed.

We assume that the amplitude a is small compared to the wavelength λ and water depth h, in the sense that $a \ll \lambda$ and $a \ll h$. These conditions allow us to linearize the problem [6]. This paper concerns incompressible fluid, this implies the continuity equation

$$\frac{D\rho}{Dt} = -\rho \nabla \cdot \mathbf{q}. \tag{1}$$

By the assumption of inviscid flow, the momentum equation can be written as

$$\frac{D\mathbf{q}}{Dt} = -\frac{1}{\rho}\nabla p + \mathbf{g}, \tag{2}$$

where p denotes pressure, $\mathbf{q}$ velocity vector, $\mathbf{g}$ gravity acceleration, ρ density, and $\frac{D}{Dt}$ material derivative.

Since the fluid is assumed ideal and the flow is irrotational, by these conditions Laplace's equation holds for the velocity potential fluid. Therefore,

$$\nabla^2 \phi = 0, \tag{3}$$

followed by boundary conditions along the surface and the bottom. The boundary conditions are given as linear case at the free surface

$$\frac{\partial \eta}{\partial t} = \frac{\partial \phi}{\partial y}, \qquad \text{at } y = h \tag{4}$$

$$\frac{\partial \phi}{\partial t} = -g\eta, \qquad \text{at } y = h \tag{5}$$

and at the bottom

$$\frac{\partial \phi}{\partial y} = 0, \qquad \text{at } y = 0. \tag{6}$$

2.2 Conditions of Computation

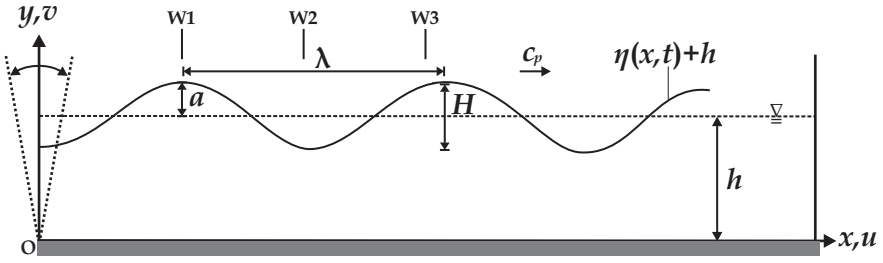

Fig. 2: Schematic diagram of numerical wave tank (NWT).

The problem formulated here is water waves propagation generated by flap type wavemaker, the schematic diagram of NWT is shown in Fig. 2. We use

Cartesian as the coordinates, a flap type wavemaker is selected as waves generator and located at $x = 0$, where the hinge of the flap type wavemaker is at the base of the tank. Wave propagating along x-axis which is perpendicular to the y-axis. In Fig. 2, a denotes wave amplitude, λ wavelength, H wave height, h water depth, η surface wave elevation, u horizontal particle velocity, v vertical particle velocity, c_p phase velocity of wave, and W_i location for wave elevation $(i = 1, 2, 3)$.

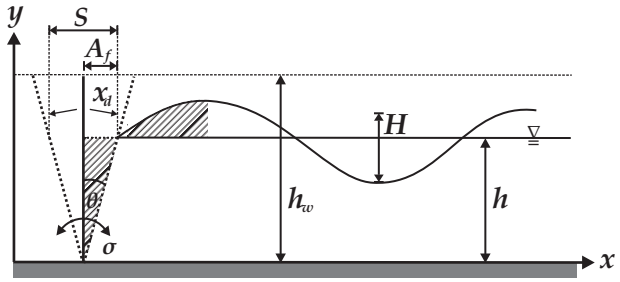

Fig. 3: Flap type wavemaker displacement.

The flap type wavemaker displacement $x = x_d(y, t)$ is given as function of time as in [1] (See Fig. 3):

$$x_d = \left(\frac{y}{h}\right) A_f \sin(\sigma t), \tag{7}$$

where x_d is flap displacement at corresponding y location on the flap and σ is the angular frequency. Flap stroke amplitude A_f and rotation angle θ are related as

$$\theta = \arctan\left(\frac{A_f}{h}\right).$$

3 Numerical Scheme

The main concepts of the SPH method were described in detail by Monaghan [7] and Liu [3]. Numerical scheme of the SPH method is used to discretize the governing equations which based on integral interpolants. Consider a function $A(\mathbf{r})$ which can be approximated by

$$A(\mathbf{r}) = \int_{\Omega} A(\mathbf{r}')W(\mathbf{r} - \mathbf{r}', h')d\mathbf{r}', \tag{8}$$

where h' is the smoothing length. This approximation can be written in discretized form involving particle-i and particle-j as

$$A_i(\mathbf{r}_i) = \sum_j A_j \frac{m_j}{\rho_j} W(\mathbf{r}_i - \mathbf{r}_j, h'), \tag{9}$$

where i and j are index of the particle, m_j mass, ρ_j density, and W smoothing kernel.

3.1 Smoothing Kernel

In this paper, we use cubic spline kernel as in [8]:

$$W(s,h') = \frac{15}{7\pi(h')^2} \begin{cases} \frac{2}{3} - s^2 + \frac{1}{2}s^3, & 0 \le s < 1 \\ \frac{1}{6}(2-s)^3, & 1 \le s < 2 \\ 0, & 2 \le s \end{cases} \tag{10}$$

where $s = |\mathbf{r}_i - \mathbf{r}_j|/h'$ is relative distance of particle-i and particle-j.

3.2 The Continuity Equation

The continuity equation is based on the conservation of mass. Writing (1) in SPH discretized form as in [9]:

$$\frac{D\rho_i}{Dt} = \sum_j m_j(\mathbf{q}_i - \mathbf{q}_j) \cdot \nabla_i W(\mathbf{r}_i - \mathbf{r}_j, h'), \tag{11}$$

where ρ_k and $\mathbf{q}_k$ are density and velocity vector of particle-k (evaluated at $k = i$ or $k = j$), respectively, and m_j is mass of particle-j.

3.3 The Momentum Equation

The momentum equation is based on the conservation of momentum. Writing (2) in SPH discretized form as in [9]:

$$\frac{D\mathbf{q_i}}{Dt} = -\sum_j m_j \Big(\frac{p_i}{\rho_i^2} + \frac{p_j}{\rho_j^2} + \Pi_{ij} \Big) \cdot \nabla_i W(\mathbf{r}_i - \mathbf{r}_j, h') + \mathbf{g}, \tag{12}$$

where p_k is pressure of particle-k (evaluated at $k = i$ or $k = j$). The artificial viscosity term Π_{ij} is added to pressure terms within the momentum equation (12). The artificial viscosity Π_{ij} has the form as in [7]:

$$\Pi_{ij} = \begin{cases} \dfrac{-\alpha c \mu_{ij} + \beta \mu_{ij}^2}{(\rho_i + \rho_j)/2}, & \mathbf{q}_{ij} \cdot \mathbf{r}_{ij} < 0 \\ 0, & \mathbf{q}_{ij} \cdot \mathbf{r}_{ij} > 0 \end{cases} \tag{13}$$

where c is the speed of sound, $\mu_{ij} = h'\mathbf{r}_{ij} \cdot \mathbf{q}_{ij}/(\mathbf{r}_{ij}^2 + \tau^2); \mathbf{r}_{ij} = \mathbf{r}_i - \mathbf{r}_j; \mathbf{q}_{ij} = \mathbf{q}_i - \mathbf{q}_j, \alpha = 0.03$, $\beta = 0$, and $\tau = 0.001$.

3.4 The Equation of State

Generally, the equation of state is used to relate pressure and density which follows

$$p = \frac{c_0^2 \rho_0}{\gamma} \left[\left(\frac{\rho}{\rho_0} \right)^{\gamma} - 1 \right], \tag{14}$$

where $\rho_0 = 1000, c_0 = c(\rho_0) = 14$, and $\gamma = 7$ are the reference density, speed of sound at the reference density, and polytropic constant, respectively. In this expression, c_0^2 also act as stiffness constant. Incompressibility can be approximated by setting high value of c_0^2.

3.5 Collision Treatment

Collision treatment is employed to constraint the particle system within well-defined boundaries. It means that while particles collide with the tank wall, they must stay inside its boundaries. Likewise, particles cannot penetrate into the object when collide with an obstacle. Collision treatment is divided into two sub parts, i.e. collision detection and collision response [10].

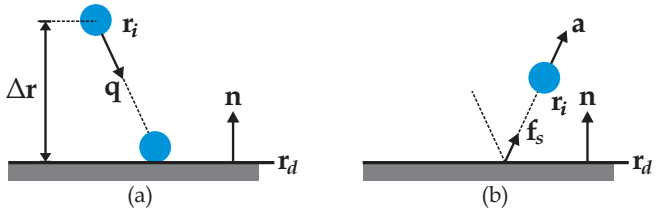

Fig. 4: Illustration of (a) Collision detection; (b) Collision response.

Collision Detection This treatment is employed by detecting wall position $\mathbf{r}_d$ and particle position $\mathbf{r}_i$, where $\Delta\mathbf{r} = \mathbf{r}_d - \mathbf{r}_i < \epsilon$. Note that ϵ is defined as very small number constant. We only consider collisions by condition $\Delta\mathbf{r} = \mathbf{r}_d - \mathbf{r}_i > \epsilon$, hence if a particle is located on the surface, it is not colliding. The illustration is shown in Fig. 4(a).

Collision Response After detecting collision between particle and wall, then collision response is employed by adding particle acceleration in appropriate with vector normal $\mathbf{n}$ of the wall. The illustration is shown in Fig. 4(b). Meanwhile, the algorithm of collision treatment is given in Algorithm 1.

Algorithm 1 Collision detection and collision response algorithms

```
for i = 1 → N do
    Δr = r_d − r_i < ϵ
    Step 1: Collision detection
    if Δr = r_d − r_i > ϵ then
        Step 2: Collision response
        f_s = (k_p Δr − k_d(n · q))n
        a_{t+Δt} = a_t + f_s
    end if
end for
```

Here, N denotes the number of particle, $\mathbf{f}_s$ spring force vector, $k_p = 2 \times 10^6$ spring constant, $k_d = 100$ damping constant, $\mathbf{q}$ particle velocity vector, $\mathbf{a}$ particle acceleration vector, and subscript t time.

4 Results and Discussion

4.1 Validation of the SPH Method

Before we proceed the study of wave propagation, the accuracy of the numerical scheme as well as the suitability of the model equations must be tested. Here, the accuracy of the presented numerical model is validated by comparing the numerical results with WMT and LWT.

Validation with WMT For flap type wavemaker, the relation between wave height, stroke length, and water depth is given as in [11] by

$$\left(\frac{H}{S}\right)_{\text{flap}} = \frac{4\sinh kh}{kh}\frac{kh\sinh kh - \cosh kh + 1}{\sinh 2kh + 2kh}. \tag{15}$$

By comparing shaded-in area in Fig. 3, ratio of the wave height to stroke length for flap type wavemaker is given as

$$\left(\frac{H}{S}\right)_{\text{flap}} = \frac{kh}{2}. \tag{16}$$

In Fig. 5(a), results from the SPH method and WMT are compared in terms of the wave height to stroke length ratio (H/S) against the wavenumber k times water depth h. A very good agreement between WMT and SPH results validates the methodology.

Validation with LWT The second validation is a comparison of generated wave to linear wave theory (LWT), which uses the linear form

$$\eta = a\cos(kx - \omega t), \tag{17}$$

where a is the wave amplitude determined by curve fitting, $\omega = 2\pi/T$ is the angular frequency of the wave, $k = 2\pi/\lambda$ is the wave number, and η is the wave elevation of the LWT wave. Here, ω and k are related by the dispersion relation $\omega \approx k\sqrt{gh}$ for shallow water wave. Fig. 5(b) shows that the wave elevation of the SPH method is identical to LWT.

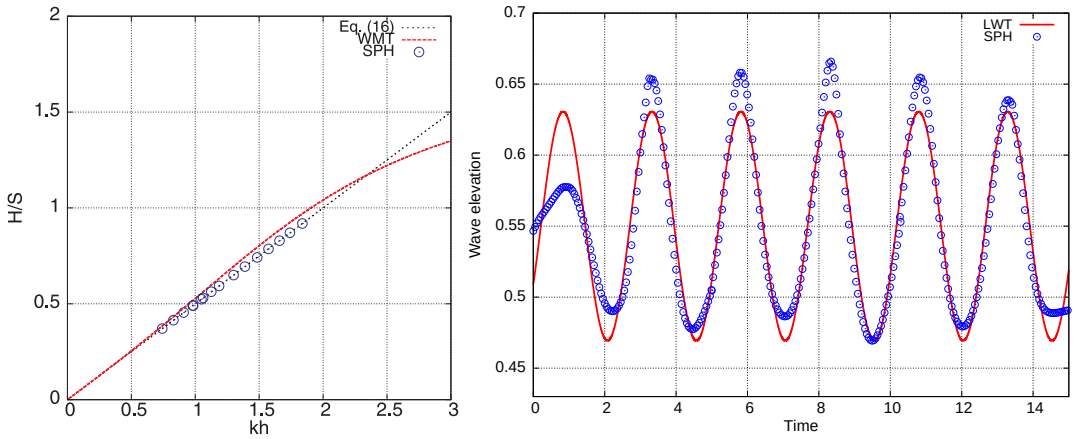

(a) (b)

Fig. 5: (a) Comparison of SPH results to wavemaker theory (WMT); (b) Comparison of wave elevation of the SPH method to LWT.

4.2 Variable of Flap Stroke Length A_f

At constant flap period T_f and water depth h, dependence of flap stroke length A_f was simulated. This simulation used 8296 particles. The time history of wave elevation for different A_f is shown in Fig. 6. The wave elevation was measured in location W1. The simulation results were compared to the analytical solutions in Table 1. Analytical wave amplitude a determined by curve fitting, while the wavelength compared to the dispersion relation for shallow water wave. The results show good agreement between numerical results and analytical solutions. A good agreement between numerical results and analytical solutions also was obtained for the changes in variable water depth and variable flap period.

Table 1: Comparison of numerical and analytical results

No.	A_f	$a_{\text{numerical}}$	$a_{\text{analytical}}$	**Error** (%)	$\lambda_{\text{numerical}}$	$\lambda_{\text{analytical}}$	**Error** (%)
1.	0.125	0.074336	0.072796	2.11	2.00041	1.989	0.57
2.	0.15	0.097927	0.081046	20.82	1.97746	1.989	0.58
3.	0.175	0.113400	0.091243	24.28	1.99892	1.989	0.49
4.	0.2	0.117853	0.098565	19.56	1.9853	1.989	0.18

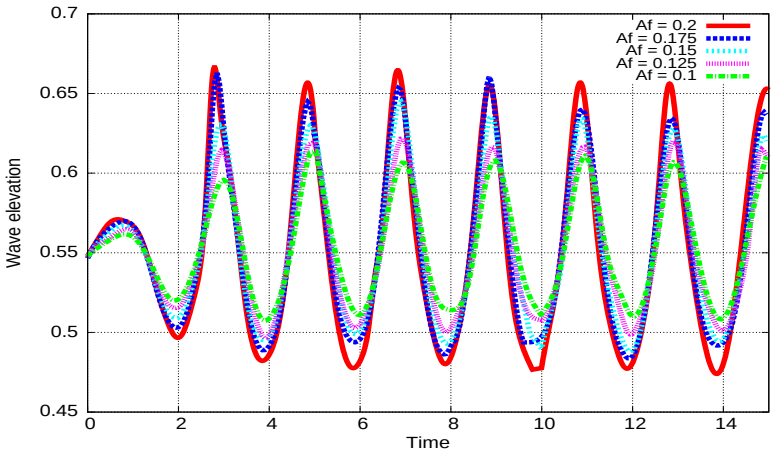

Fig. 6: Time history of wave elevation for different A_f.

Dependence of flap stroke length A_f to wave amplitude is shown in Fig. 7(a). The result shows that the wave amplitude increases as increase flap stroke length A_f. Dependence of flap stroke length A_f to wavelength is shown in Fig. 7(b). It has been observed that the wavelength relatively constant for different flap stroke length. These results were verified with dispersion relation LWT for shallow water wave.

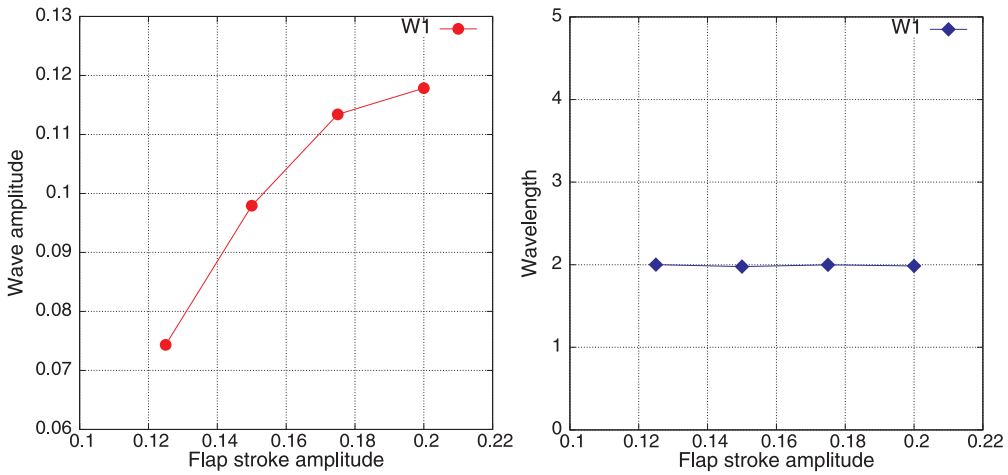

Fig. 7: (a) Flap stroke length A_f vs. wave amplitude a; (b) flap stroke length A_f vs. wavelength λ.

4.3 Variable of Flap Period T_f

At constant flap stroke length A_f and water depth h, dependence of flap period T_f was simulated. This simulation used 8296 particles. The time history of wave elevation for different T_f is shown in Fig. 8(a). The wave elevation was measured in location W1. The relation between flap period T_f and wave period is shown in Fig. 8(b). It has been observed that wave period is directly proportional to flap period T_f.

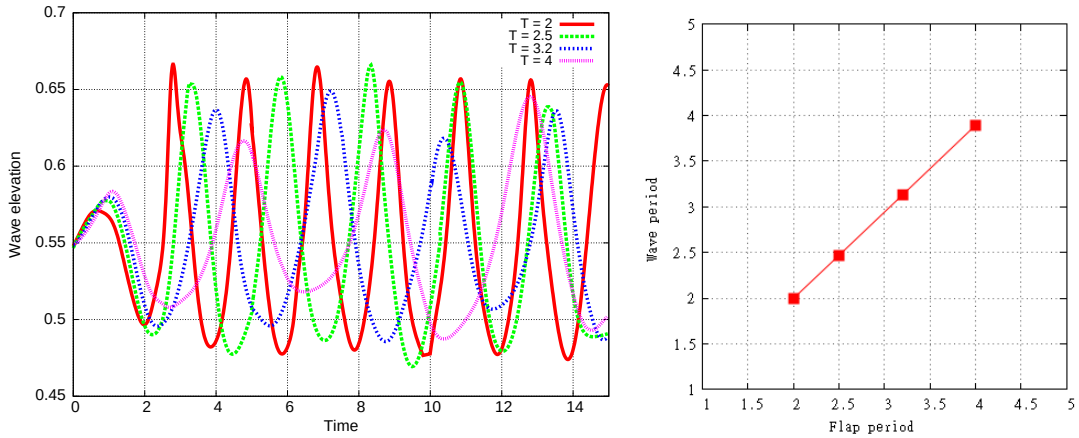

(a) (b)

Fig. 8: (a) Time history of wave elevation for different T_f; (b) Flap period T_f vs. wave period T.

Dependence of flap period T_f to wave amplitude and wavelength is shown in Fig. 9(a) and (b), respectively. Fig. 9(a) gives the information that maximum wave amplitude was obtained by certain flap period T_f and gives fluctuated value for the other certain flap period T_f. This means that any choice of flap period T_f cannot be able to form the desired wave. Meanwhile in Fig. 9(b) shows that wavelength increases as increase in flap period T_f. These result were verified by dispersion relation LWT for shallow water wave.

4.4 Variable of Water Depth h

At constant flap stroke length A_f and flap time period T_f, the effect of changing water depth h was simulated. The wave elevation was measured in location W1. The simulation results are shown in Fig. 10(a) and (b), related to wave amplitude and wavelength, respectively. The results show that both wave amplitude and wavelength increases as increase water depth h.

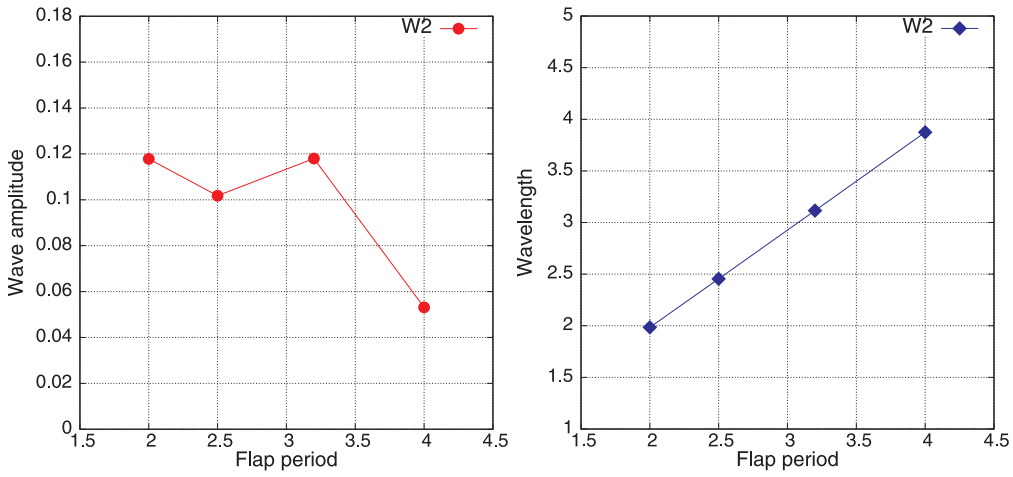

(a) (b)

Fig. 9: (a) Flap period T_f vs. wave amplitude a; (b) flap period T_f vs. wavelength λ.

4.5 Variable of Slope

In this study, a sloped tank is introduced to damp out the waves. This technique also used by Lal and Elangovan [1] and Finnegan and Goggins [2]. At constant flap stroke length A_f, flap period T_f, and water depth h, we consider various slopes with ratio 1:2, 1:3, and 1:4. The comparison of wave elevation in location W1 and W4 is shown in Fig. 11(a).

The measured wave elevation for various slopes in location W4 are plotted in Fig. 11(b). It is obvious to see that damping of the wave has occurred as a result of the sloped tank. Here, the slope for ratio 1:2 is effectively damped the wave elevation.

5 Conclusion

A numerical scheme of wave propagation generated by flap type wavemaker was simulated using the SPH method. The numerical results of the SPH method were compared to wavemaker theory and linear wave theory in order to validate the model. A good agreement results validated the methodology. Characteristics and wave profiles were studied by varying the governing parameters, i.e. flap stroke length dependence, flap period dependence, water depth dependence, and varying slope ratio. A comparison between the numerical results and the analytical solutions was undertaken to ensure the accuracy of the model. The numerical results show a good agreement with the analytical solutions.

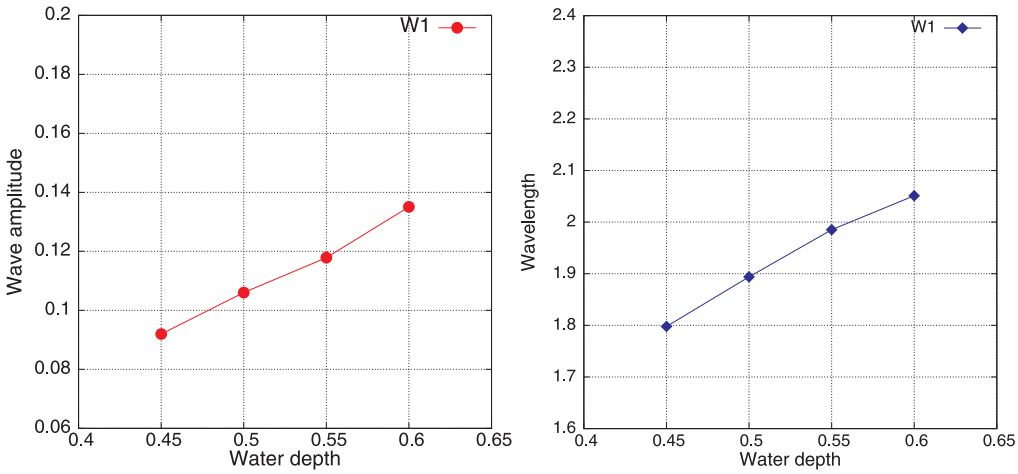

(a) (b)

Fig. 10: (a) Water depth h vs. wave amplitude a; (b) Water depth h vs. wavelength λ.

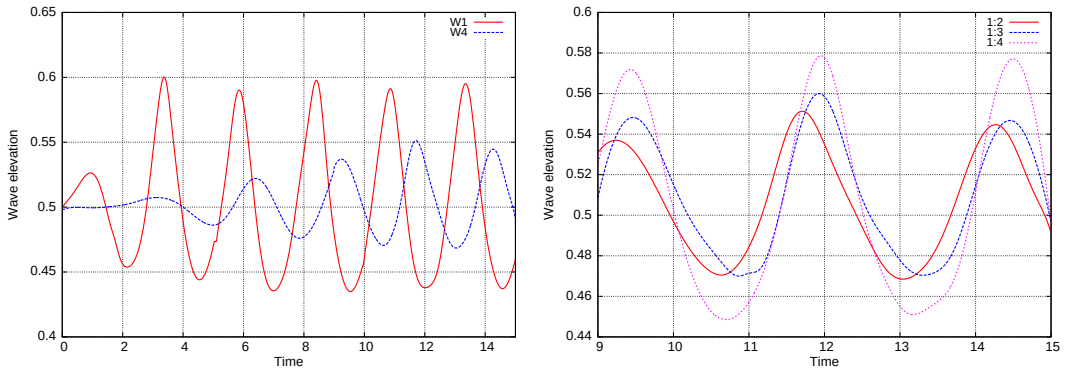

(a) (b)

Fig. 11: (a) Time history of wave elevation in location W1 and W4 for ratio 1:2; (b) A comparison of wave elevation for different slope ratio.

References

1. Lal, A., Elangovan, M.: CFD simulation and validation of flap type wave-maker, *World Academy of Science, Engineering and Technology*, **46**, 76-82 (2008).
2. Finnegan, W., Goggins, J.: Numerical simulation of linear water waves and wave-structure interaction, *Ocean Engineering*, **43**, 23-31 (2012).
3. Liu, G. R., Liu, M. B.: *Smoothed particle hydrodynamics: a meshfree particle method*, World Scientific Publishing Co. Pte. Ltd, Singapore (2003).
4. Lucy, L. B.: A numerical approach to the testing of the fission hypothesis, *Astron. J*, **82**, 1013-1024 (1977).
5. Gingold, R. A., Monaghan, J. J.: Smoothed particle hydrodynamics: theory and application to non-spherical stars. *Mon. Not. R. Astr. Soc*, **181**, 375-389 (1977).
6. Kundu, P. K., Cohen, I. M.: *Fluid mechanics (second edition)*, Academic Press, United States of America, 199-211 (2002).
7. Monaghan, J. J.: Smoothed Particle Hydrodynamics, *Annu. Rev. Astron. Astrophys*, **30**, 543-574 (1992).

8. Monaghan, J. J., Lattanzio, J. C.: A refined method for astrophysical problems, *Astron. Astrophys*, **149**, 399-406 (1985).
9. Monaghan, J. J.: Simulating free surface flows with SPH, *Journal of Computational Physics*, **110**, 399-406 (1994).
10. Kelager, M.: *Lagrangian fluid dynamics using Smoothed Particle Hydrodynamics*, Department of Computer Science, University of Copenhagen, Denmark, 8-28 (2006).
11. Dean, R. G., Dalrymple, R. A.: *Water wave mechanics for engineers and scientists*, World Scientific Co. Pte. Ltd, Singapore, 170-178 (1991).